A. Świerczyńska, J. Łabanowski, D. Fydrych

Effect of Linear Energy and Microstructure on the Content of Residual Hydrogen in Welded Joints made of Superduplex Steels

Abstract: The article presents tests concerning the content of retained hydrogen present in FCAW and SAW welded joints made of superduplex steel. The use of various welding processes resulted in the obtainment of welds having different microstructures and ferrite contents. Measurements of retained hydrogen present in joints (performed using the complete combustion method) revealed various contents of hydrogen in the base material and in the welds subjected to the tests. It was determined that the content of hydrogen in welds made of superduplex steels depends not only on the volumetric content of microstructures but also on their composition and welding heat input.

Keywords: superduplex stainless steel, FCAW, SAW, weldability, residual hydrogen

DOI: *10.17729/ebis.2016.5/22*

Introduction

Duplex ferritic-austenitic steels have a two-phase structure containing approximately 50% of each phase. The unique structure is obtained by using an appropriate chemical composition and manufacturing process [1,2]. In comparison with "classical" duplex steels, superduplex steels are characterised by higher chromium, nickel, nitrogen and molybdenum contents. The above-presented chemical elements are responsible for the stability of phases during welding, and, at the same time, for excellent corrosion resistance and enhanced mechanical properties. Duplex steels can be used in warm sea water environments, having significant chlorine contents, and in acidic chloride media. The practical applications of duplex steels include the output and processing of oil and gas, heat exchangers in chemical and petrochemical industries and structures operated in tropical sea environments. The weldability of presently manufactured duplex steels can be limited by several factors such as the improper ratio of phases α/γ in the weld and HAZ, the segregation of alloying elements between both phases leading to the formation of micro-areas depleted in Cr and Mo, the precipitations of nitrides and intermetallic phases, the escape of nitrogen from root runs, and the presence of oxide layers on joint surfaces [3-5]. The effect of the above named factors is primarily dependent on the chemical composition of base materials and filler metals as well as on welding thermal cycle parameters.

dr inż. Aleksandra Świerczyńska (PhD (DSc) Eng.), dr hab. inż. Jerzy Łabanowski (PhD (DSc) hab. Eng.), Professor at Gdańsk University of Technology; dr inż. Dariusz Fydrych (PhD (DSc) Eng.) – Gdańsk University of Technology; Faculty of Mechanical Engineering

Hydrogen can penetrate liquid or solid metallic materials. In the metallurgy of welding processes, hydrogen is divided into potential hydrogen, diffusible hydrogen, retained (residual) hydrogen and total hydrogen, constituting the sum of diffusible and retained hydrogen [6]. Retained hydrogen accumulates, in both atomic and molecular forms, in empty spaces; its removal from joints requires long desorption in vacuum at a temperature of approximately 900 K [7].

The relocatability of hydrogen in steel microstructure depends on diffusivity. Test results [8] reveal that the hydrogen diffusion coefficient (at a temperature of 25°C) in austenitic steel AISI 316L amounts to $3.1 \cdot 10^{-16}$ $m^2 \cdot s^{-1}$, whereas in ferritic steel AL 29-4-2 amounts to $1.1 \cdot 10^{-11}$ $m^2 \cdot s^{-1}$. As can be seen, the hydrogen diffusion coefficient is by five orders of magnitude higher in ferritic steels than in austenitic steels. However, it should be noted that the solubility of hydrogen in austenite is by approximately two orders of magnitude higher than in ferrite.

Because of the anisotropic microstructure of duplex steels, the relocatability of hydrogen in these steels depends on the orientation of phases. Works [9,10] state that the diffusion coefficient is higher if the stream of hydrogen is parallel to elongated grains, yet the difference in relation to the perpendicular direction in relation to grains is only two-fold. The morphology of austenite grains is also important as more dispersed grains favour the extension of hydrogen diffusion paths and increased amounts of trapped hydrogen in comparison with equiaxial grains separated by wide ferritic bands [11]. The shape of austenite grains in the microstructure significantly affects the properties of duplex steels. Crack resistance requires slight gaps between grains of ductile austenite. Tests [12] revealed that elongated austenite grains oriented perpendicularly in relation to the direction of load effect reduce the risk of hydrogen-induced crack formation in duplex steels. Hydrogen entering the material during welding becomes trapped in the microstructure of duplex steels during solidification; significant amount of hydrogen remain in austenite [13]. Tests performed by Kacar [14] indicate that the amount of potential hydrogen in a weld, made using various electrodes providing various amounts of ferrite and austenite in the structure, is similar.

Tests

The objective of the tests was to determine the content of retained hydrogen in welded joints made of superduplex steel using the FCAW and SAW methods and correlating the hydrogen content with the structure of joints and heat input. The scope of the tests involved metallographic tests, measurements of ferrite contents in the microstructure, hardness tests and measurements of retained hydrogen amounts.

The tests involved 13 mm thick plates made of superduplex steel URANUS 52N+ (1.4507, PN-EN 10027: X2CrNiMoCuN25-6-3, UR 52N+) in the solution annealed state. The chemical composition of the steel is presented in Table 1. In comparison with basic duplex steel 2205, the steel subjected to the tests was characterised by increased contents of chromium, nickel, nitrogen, molybdenum and copper. As a result, the steel was characterised by high corrosion resistance; its pitting corrosion index (PREN) amounted to 40.9. The FCAW process was performed using a PREMIARC DW-25-94 rutile flux-cored (ASME AWS A5.22: E2594T1-1/4) KOBELCO

Table 1. Chemical composition of steel URANUS 52N+ and electrode wires used in the tests

Material designation	C	Si	Mn	Cr	Ni	Mo	Cu	N
URANUS 52N+	0.03	0.26	0.86	25.1	5.8	3.5	1.4	-
PREMIARC DW-25-94	0.03	0.5	1.18	25.7	9.6	3.8	<0.1	0.24
LNS Zeron 100X	0.02	0.3	0.7	25.0	9.3	3.7	0.6	0.23

having a diameter of 1.2 mm and a gas shielding mixture of Ar + 18% CO_2 (PN-EN 14175: M21). The SAW process was performed using an LNS Zeron 100X (ASME AWS A5.9/A5.9M: ER 2594) Lincoln Electric solid wire having a diameter of 2.4 mm and low-hydrogen flux (EN 760: A AF2 63 AC H5) [15].

Joints were prepared in accordance with PN-EN ISO 15614-1. The edges of plates were subjected to milling and, directly before welding, to cleaning performed using an angle grinder. The pre-weld edge preparation manner is presented in Figure 1.

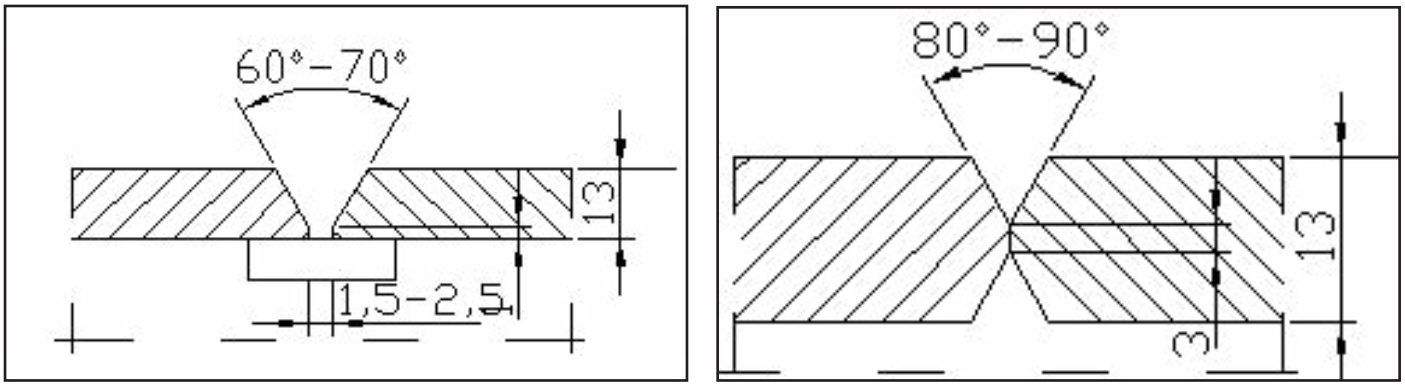

Fig. 1. Preparation of plate edges for a) FCAW and b) SAW [15]

The FCAW joint was made as single-sided using a ceramic backing strip. The weld consisting of 4 layers was made using 5 runs. The process of welding was performed maintaining interpass temperature below 100°C. The weld temperature was measured using a photoelectric pyrometer. After making a subsequent run, the surface of the previously made run was cleaned by grinding. The SAW joints were welded in a flat positon with the electrode positioned vertically; the electrode extension amounted to 25 mm. The double-sided weld was made using 2 runs, maintaining interpass temperature below 100°C.

During the FCAW process, the welding heat input amounted to, on average, 0.98 kJ/mm, whereas during the SAW process, the welding heat input amounted to, on average, 2.13 kJ/mm. The thermal efficiency coefficient adopted during the tests amounted to k=0.8 and k=1 respectively (in accordance with PN-EN 1011). After welding, the joints were subjected to non-destructive tests, i.e. visual tests (VT), penetrant tests (PT) and radiographic tests (RT). The imperfections detected in the welded joints did not exceed permissible values specified for quality level B according to PN-EN ISO 5817.

The metallographic tests were performed using a Neophot – 32 light microscope. The specimens were etched using Beraha's (HCl + $K_2S_2O_4$) and Marble's ($CuSO_4$ + HCl + H_2O) reagent. The determination of the volume fraction of phases in the welds was performed using a Fisher MP30 ferroscope. The measurements were performed on the cross-sections of the specimens in 3 lines: from the weld face side, in the central line and from the weld root side. The hardness measurements of the welded joints were performed in accordance with PN-EN ISO 9015-1 using a Vickers-Brinell HPO-250 hardness tester. The measurements were based on the Vickers hardness test performed in accordance with PN-EN 6507 under a load of 49 N (HV5). Indentations were made in three measurement lines passing through the base material, HAZ and the weld of each specimen. The first and third lines were located 2 mm away from the plate surface, whereas the second line was located in the centre of the joints and in parallel to lines 1 and 3.

The contents of retained hydrogen in the welded joints were determined using an ONH836 analyser manufactured by LECO. The analyser can be used for identifying the contents of hydrogen, oxygen and nitrogen in inorganic

materials, including iron alloys, non-ferrous metal alloys and ceramics [16]. In terms of hydrogen, the measurement range is restricted between 0.1 ppm and 2500 ppm for a 1 g heavy specimen, whereas accuracy amounts to 0.05 ppm or 2% of a result obtained. The measurements were performed on specimens (3 mm × 3 mm × 5 mm) cut out of the base material and of welds.

Test Results

Metallographic Tests

The macroscopic metallographic tests revealed the proper cross-sectional geometry of the joints (Fig. 2). Both the FCAW and SAW joints were characterised by metallic ductility, as well as by the lack of cracks, undercuts and other welding imperfections.

The detailed microscopic metallographic tests involved the welds and HAZ areas of the joints. The base material of steel URANUS 52N+ revealed a band-like structure containing austenite areas, elongated in the direction of rolling, visible against the background of ferrite (Fig. 3); such a structure is characteristic of rolled products.

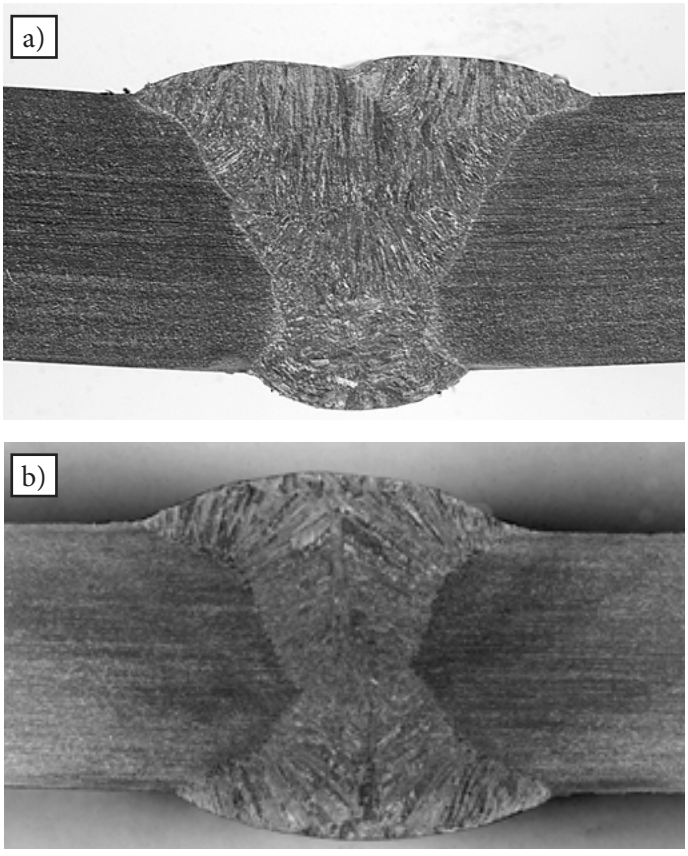

Fig. 2. Macroscopic image of the joints made of steel URANUS 52N+ a) FCAW and b) SAW [17]

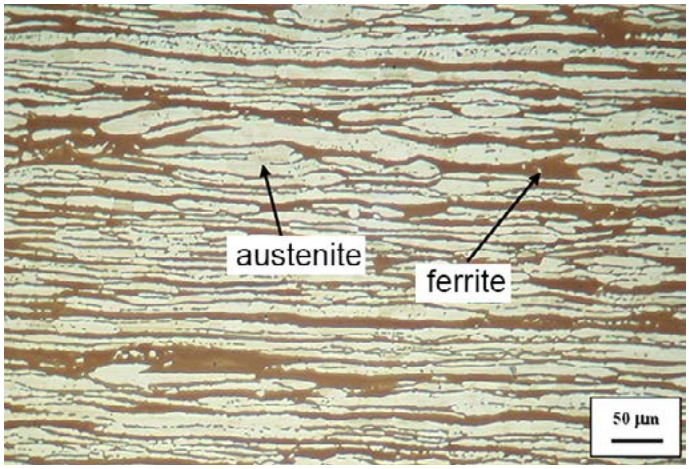

Fig. 3. Structure of the base material of steel URANUS 52N+; mag. 250× [17]

The microstructures of the SAW and FCAW welds made using various values of welding heat input are presented in Figure 4. Figure 4b (FCAW joint) reveals differences in the structure of the face, centre and root areas of the weld. Bright austenite precipitations, visible against the dark ferritic matrix, can be divided into (I) acicular austenite precipitations oriented along dendritic boundaries of ferrite grains, (II) austenite precipitations inside ferrite grains and (III) austenite precipitations in the Widmanstätten patterns, i.e. so-called secondary austenite (γ_2), formed as a result of secondary thermal cycles.

After solidification, the weld, below the temperature of solidus, revealed a purely ferritic structure. The further decrease in temperature was accompanied by the transformation $\alpha \rightarrow \alpha+\gamma$. The transformation started at a temperature of approximately 1300°C [18] and its kinetics depended and were controlled by the diffusion of alloying components. Time during which the weld material was affected by temperature, restricted within the range of temperature corresponding to the presence of ferritic structure, depended on heat input during welding. The longer the hold time at high temperature, the greater the tendency of grain growth – such

a trend was also observed in the test joints. The columnar ferrite dendrites present in the weld of the FCAW joints, welded using low heat input, were smaller in comparison with the columns of ferrite present in the weld of the SAW joint (Fig. 4).

Below a temperature of 1300°C it was possible to observe the growth of phase γ, nucleating on the boundaries of ferrite grains and expanding to match the shape of the grains and create a continuous lattice. The limited growth of austenite in the direction perpendicular to the boundaries of ferrite grains resulted from the limited diffusion of alloying components along the non-coherent boundary. The nucleation inside ferrite grains was facilitated by numerous crystalline structure defects.

Secondary austenite $\gamma 2$ appeared in the microstructure of the weld and of the HAZ after heating up to a temperature below 1300°C. The process was connected with the high thermodynamic instability of alloy ferrite at higher temperatures. The secondary austenite was present both on the boundaries of grains α and within the ferrite grains. The clusters of phase $\gamma 2$ revealed the structure having the Widmanstätten pattern; the clusters were formed as a result of diffusible transformation.

The FCAW weld (Fig. 4.b) revealed a significant increase in austenite content in the centre of the weld and in the weld root, which was connected with the formation of secondary austenite $\gamma 2$ as a result of the effect of a complex welding thermal cycle. In the SAW weld, an increase in austenite content through the formation of $\gamma 2$ was observed only in the centre of the weld. In the two-run weld, the thermal effect of the second run did not trigger any structural changes in the weld face (run no. 1).

The visual analysis of the microstructures presented in Figure 4 revealed significantly greater amounts of ferrite in the SAW welds than in those made using the FCAW method.

Table 2 presents the percentage volume fraction of ferrite in the test welds. The average content of ferrite in the base material amounted to 46.9%. In the FCAW weld, the content of ferrite ranged from, on average, 44% in the face, through 43% in the centre of the joint, to 38% in the root. The weld of the joint made using

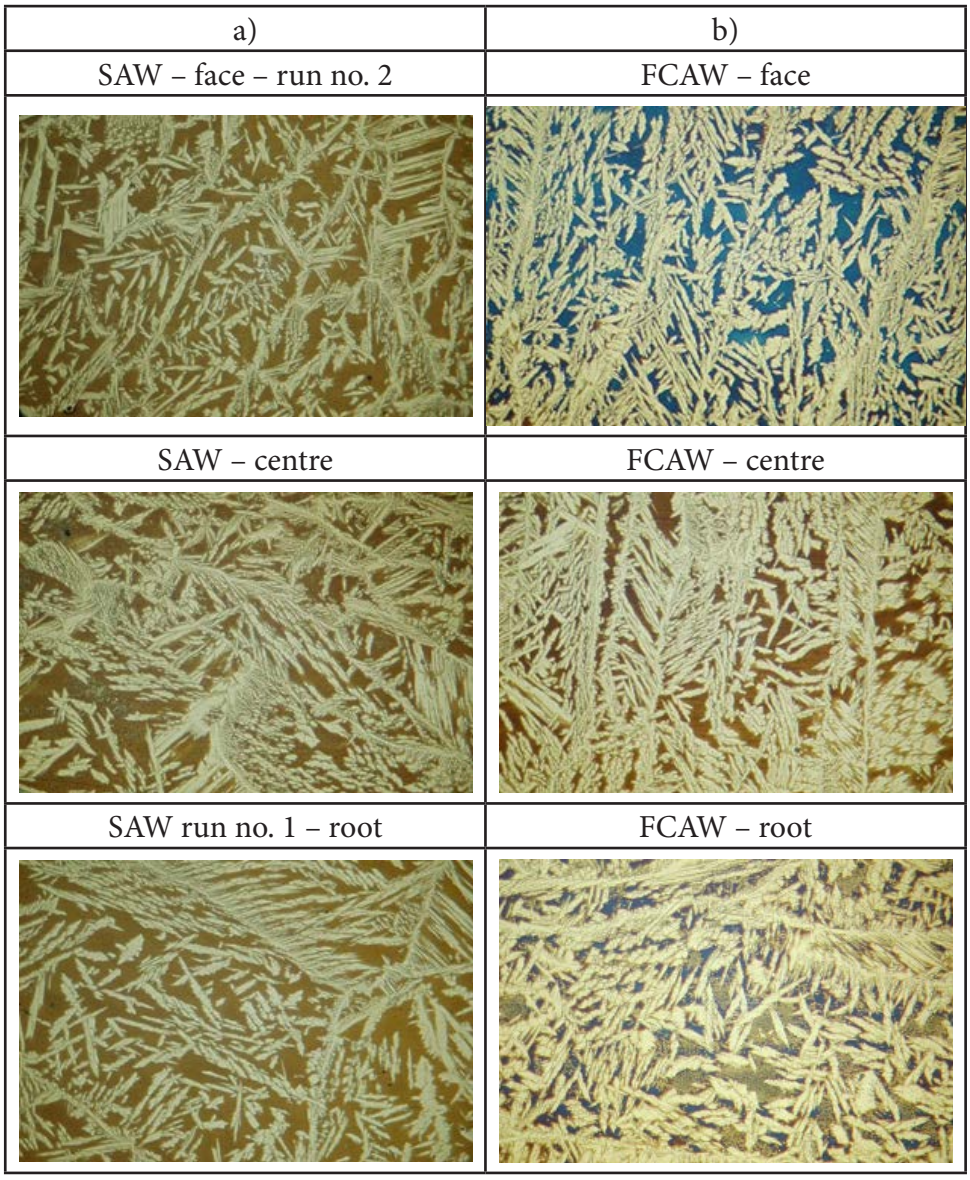

Fig. 4. Microstructures of the welds in the welded joints a) SAW, b) FCAW [17]

the SAW method was characterised by the highest ferrite content amounting to 57% in the entire cross-section.

Table 2. Volume fraction of ferrite in steel URANUS 52N+ and in the welds of the joints made using the FCAW and SAW methods [17]

BM		
46,9%		
FCAW		
Weld face	Weld centre	Weld root
44.4%	43.2%	37.5%
SAW		
Weld face 1	Weld centre	Weld root 2
57.0%	57.1%	57.4%

Figure 5 presents the distribution of cross-sectional hardness of the test welded joints. The joint made using the FCAW method was characterised by the discrepancy of hardness measurement results (Fig. 5a). A significant increase in weld hardness, in comparison with that of the base material, was observed along all measurement lines. In the weld, the average hardness amounted to 282 HV5, whereas in the base material it amounted to 263.5 HV5. The most important hardness values (up to 291 HV5) were observed in the face layer of the weld. Such hardness distribution was correlated with the higher ferrite content in the weld face, which was characterised by hardness higher than that of the austenitic phase [19]. The hardness in the HAZ of the joint made using the FCAW method was between the hardness of the weld and that of the base material.

In the SAW welded joint the cross-sectional hardness did not vary significantly, amounting to between 260 and 283 HV5 in the entire joint (Fig. 5b). The only area characterised by slightly higher hardness was the HAZ of the joint, which was connected with the increased content of ferrite in this area [17]. Differences in hardness values of the joints made using the FCAW and SAW methods could also result from various grades of weld deposits used during welding.

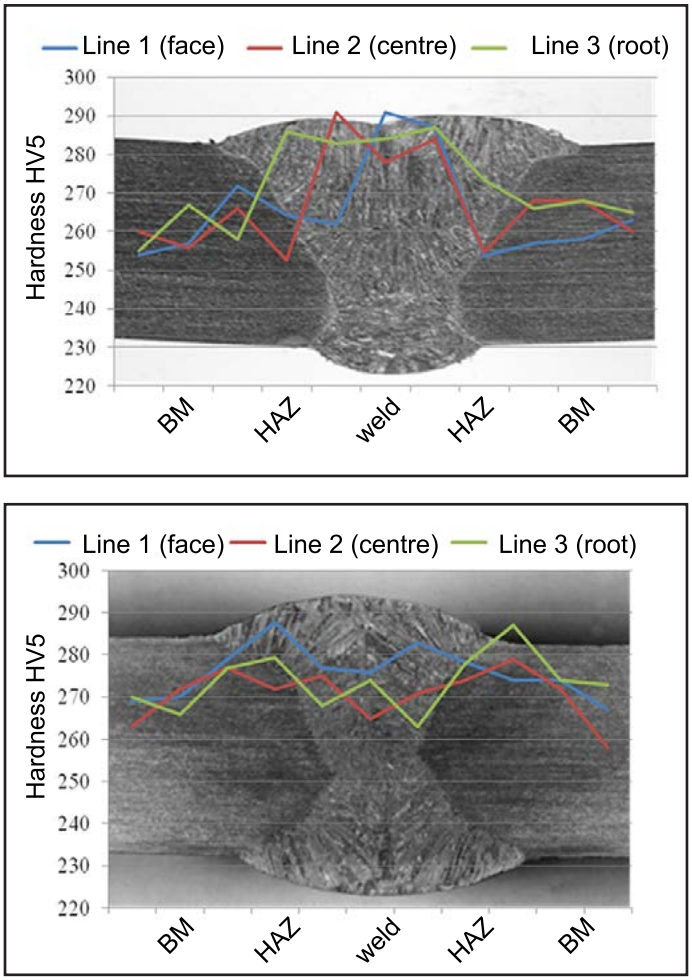

Fig. 5. Distribution of hardness HV5 in the joints made using a) FCAW and b) SAW

The tests performed using an analyser manufactured by LECO enabled measurements of contents of hydrogen residual in the base material and weld specimens. Because of its narrow width, the measurements could not be performed in the HAZ of the joints. The base material of steel UR52N+ was characterised by a hydrogen content of 8.38 ppm (Table 3). The metal of the SAW and FCAW-made welds was characterised by lower hydrogen contents, which indicated properly adjusted welding parameters.

The increased content of hydrogen in the microstructure of chromium steels could lead to hydrogen brittleness and was attributed to the greater ferritic phase content. The tests revealed a greater content of hydrogen in the SAW weld, having a lower ferritic phase content than that observed in the FCAW weld. However, it is necessary to take into consideration the greater number of thermal cycles during the welding of

the joint made using the FCAW method (5 runs) and the possibility of hydrogen desorption.

The tests revealed that it is not possible to determine the simple dependence between the content of hydrogen in the weld and its microstructure. In addition to the content of ferrite in the microstructure of duplex steels, the amount of total hydrogen can also be affected by phase morphology, size of grains and amount of defects as well as the use of welding thermal cycles [12, 20].

Table 3. Results of measurement concerning the content of residual hydrogen in the base material and in the welds of the joints made using FCAW and SAW

Hydrogen content, ppm					
BM		FCAW WELD		SAW WELD	
8.66	8.38	3.25	3.59	7.96	6.97
8.47		3.89		6.56	
8.02		3.63		6.39	

Summary

The welding of superduplex steel URANUS 52N+ using the FCAW and SAW methods enabled the obtainment of proper welded joints free from cracks and precipitations of intermetallic phases. The imperfections present in the joints did not exceed permissible values specified for quality level B according to PN-EN ISO 5817.

The content of ferrite in the FCAW weld was lower, whereas the content of ferrite in the SAW weld was higher than that in the base material. In neither joint did the content of ferrite exceed maximum values considered as hazardous due to the deterioration of corrosion resistance and mechanical properties. In addition, no significant differences as to the hardness of the HAZ and welds in the test joints were found.

The content of residual hydrogen in superduplex steel URANUS 52N+ did not exceed 9 ppm. The sources of hydrogen were technological steel treatment and production processes. The content of hydrogen in the welds was lower, i.e. it amounted to approximately 3.6 ppm in the FCAW weld and to 7 ppm in the SAW weld.

The results revealed that the welding of superduplex steels performed using the FCAW and SAW methods as well as properly adjusted parameters and properly selected filler metals resulted in the reduction of hydrogen content in the weld. The extent of the change depended on several strongly correlated factors including chemical compositions, types of microstructures and their volume fractions as well as welding heat input.

References

[1] Lo K. H., Shek C H, Lai J. K.: *Recent developments in stainless steels.* Materials Science and Engineering – Reports, 2009, 65 (4), pp. 39-104 http://dx.doi.org/10.1016/j.mser.2009.03.001

[2] Nilsson J. O.: *Super duplex stainless steels.* Materials Science and Technology, 1992, 8 (8), pp. 685-700 http://dx.doi.org/10.1179/mst.1992.8.8.685

[3] Petterson C., Fager S.: *Welding practice for the Sandvik duplex stainless steels SAF 2304, SAF 2205 and SAF 2507.* Sandvik Steel AB, S-91-57-ENG

[4] Pramanik A., Littlefair G., Basak A. K.: *Weldability of duplex stainless steel.* Materials and Manufacturing Processes, 2015, 30 (9), pp. 1053-1068 http://dx.doi.org/10.1080/10426914.2015.1019126

[5] Prokop K., Rogalski G.: *Cold cracking susceptibility of joints made of ferritic-austenitic duplex steel 2205 during underwater wet welding.* Biuletyn Instytutu Spawalnictwa, 2016, no. 2, pp. 35-42 http://dx.doi.org/10.17729/ebis.2016.2/4

[6] Fydrych D., Łabanowski J.: *An experimental study of high-hydrogen welding processes.* Revista de Metalurgia, 2015, 51 (4), pp. 5-6 http://dx.doi.org/10.3989/revmetalm.055

[7] Woodtli J., Kieselbach R.: *Damage due to hydrogen embrittlement and stress corrosion cracking.* Engineering Failure Analysis, 2000, 7 (6), pp. 427-450 http://dx.doi.org/10.1016/s1350-6307(99)00033-3

[8] Pering T., Altstetter C.: *Comparison of hydrogen gas embrittlement of austenitic and ferritic stainless steels.* Metallurgical Transactions A, 1987, 18 (1), pp. 123-134 http://dx.doi.org/10.1007/bf02646229

[9] Mente T., Bollinghaus T.: *Modeling of hydrogen distribution in a duplex stainless steel.* Welding in the World, 2012, 56 (11-12), 66-78 http://dx.doi.org/10.1007/bf03321397

[10] Young M. C., Chan S. L., Tsay L. W., Shin C. S.: *Hydrogen-enhanced cracking of 2205 duplex stainless steel welds.* Materials Chemistry and Physics, 2005, 91 (1), pp. 21-27 http://dx.doi.org/10.1016/j.matchemphys.2004.10.042

[11] Olden V., Thaulow C., Johnsen R.: *Modelling of hydrogen diffusion and hydrogen induced cracking in supermartensitic and duplex stainless steels.* Materials & Design, 2008, 29 (10), pp. 1934-1948 http://dx.doi.org/10.1016/j.matdes.2008.04.026

[12] Woollin P., Gregori A.: *Avoiding hydrogen embrittlement stress cracking of ferritic austenitic stainless steels under cathodic protection.* ASME 23rd International Conference on Offshore Mechanics and Arctic Engineering, American Society of Mechanical Engineers, January 2004, pp. 777-784 http://dx.doi.org/10.1115/omae2004-51203

[13] Dabah E., Kannengiesser T., Mente T., Beyer K., Brauser S.: *Quantification of hydrogen effective diffusion coefficients and effusion behavior in duplex stainless steel weld metals.* Welding in the World, 2013, 57 (4), pp. 561-567 http://dx.doi.org/10.1007/s40194-013-0051-5

[14] Kaçar R.: *Effect of solidification mode and morphology of microstructure on the hydrogen content of duplex stainless steel weld metal.* Materials & Design, 2004, 25 (1), pp. 1-9 http://dx.doi.org/10.1016/s0261-3069(03)00169-9

[15] Świerczyńska A., Łabanowski J., Fydrych D.: The effect of welding conditions on mechanical properties of superduplex stainless steel welded joints. Advances in Materials Science, 2014, 14 (1), pp. 14-23 http://dx.doi.org/10.2478/adms-2014-0002

[16] http://www.leco.com/

[17] Świerczyńska A.: *Niszczenie wodorowe złączy spawanych ze stali ferrytyczno-austenitycznych typu superdupleks.* PhD. Thesis. Politechnika Gdańska 2015

[18] Liljas M.: *The welding metallurgy of duplex stainless steel.* Duplex Stainless Steel, Glasgow, Scotland, 13-16 November 1994

[19] Gadelrab K. R., Li G., Chiesa M., Souier T.: *Local characterization of austenite and ferrite phases in duplex stainless steel using MFM and nanoindentation.* Journal of Materials Research, 2012, 27 (12), pp. 1573-1579 http://dx.doi.org/10.1557/jmr.2012.99

[20] Luu W. C., Liu P. W., Wu J. K.: *Hydrogen transport and degradation of a commercial duplex stainless steel.* Corrosion Science, 2002, 44 (8), pp. 1783-1791 http://dx.doi.org/10.1016/s0010-938x(01)00143-3